RSC Advances

ROYAL SOCIETY OF CHEMISTRY

www.rsc.org/advances

Homochiral luminescent lanthanide dinuclear complexes derived from a chiral carboxylate

He-Rui Wen,*[a] Xin-Rong Xie,[a] Sui-Jun Liu,[a] Jun Bao,[a] Feng-Feng Wang,[c] Cai-Ming Liu*[b] and Jin-Sheng Liao[a]

A new family of homochiral lanthanide dinuclear complexes based on a chiral carboxylate, namely [Ln(*R*-pba)₃(phen)]₂ (Ln = La (**1**), Ce (**2**), Pr (**3**), Nd (**4**), Sm (**5**), Eu (**6**), Gd (**7**), Tb (**8**), Dy (**9**) and Ho (**10**), *R*-pba = (*R*)-2-phenylbutyric acid, phen = 1,10-phenanthroline), have been synthesized and structurally characterized by single-crystal X-ray diffraction, elemental analyses and IR spectra. Complexes **1**–**10** are isostructural and crystallize in the chiral space group $P2_1$. Their optical activity and enantiomeric nature were confirmed by the circular dichroism spectra. Complexes **6**, **8** and **9** exhibit strong fluorescent emissions with typical narrow emission bands of lanthanide ions and **6** and **8** display relatively high quantum yields. Magnetic investigations revealed that the weak antiferromagnetic exchange and/or the depopulation of the Ln(III) excited Stark sub-levels exist in **7**–**10**.

Introduction

The carboxylate-based complexes have been extensively investigated in the past decade due to their oxygen-rich donor compositions, great variety of binding modes and the possibility of offering interesting functions,[1] which includes magnetism,[2] photoluminescence,[3] molecular adsorption,[4] nonlinear optics,[5] catalysis[6] and so on. Recently, considerable attention has been focused on the lanthanide complexes based on carboxylates,[7] because the lanthanide (Ln) ions have unique electronic shell structures to meet the requirements of optical, electrical and magnetic materials, and they have strong high affinity for the oxygen atoms and can readily link different carboxylates to construct some novel oligomers or aggregates with unexpected structures and properties.[7b,7c] Although there are some reports on the preparation and properties of homochiral Ln(III) complexes based on the chiral carboxylates, the study of homochiral Ln(III) complexes attracts much more attention.[8] It is great significance of the study on chirality and related issues for the life sciences and materials science.[9] If chirality was introduced into the molecule in crystalline state,

1

the interesting multifunctional materials would be obtained,[10] which can find applications in many research areas such as enantioselective separation,[11] enantioselective synthesis,[12] asymmetric catalysis,[13] chiral magnets[14] and chiral luminescence materials.[15] Recently, we chose (*R*)-(-)-2-Phenylbutyric acid (*R*-pba) as the chiral source and 1,10–phenanthroline (phen) as the co-ligand to construct monochiral lanthanide complexes (Scheme 1). Herein, we describe the syntheses, crystal structures, circular dichroism spectra, magnetic properties and luminescent properties of a new family of homochiral dinuclear lanthanide Ln(III) complexes, namely [Ln(*R*-pba)$_3$(phen)]$_2$ (Ln = La (**1**), Ce (**2**), Pr (**3**), Nd (**4**), Sm (**5**), Eu (**6**), Gd (**7**), Tb (**8**), Dy (**9**) and Ho (**10**)).

(Insert Scheme 1)

Experimental

Materials and methods

All chemicals were of reagent grade and used as purchased without further purification. Elemental analysis (C, H and N) was performed on a Perkin-Elmer 240C analyzer (Perkin-Elmer, USA). IR spectra were measured in the range of 400–4000 cm^{-1} on a Bruker ALPHA FT-IR spectrometer using KBr pellets (Bruker, German). The circular dichroism spectra were recorded on a JASCO J-1500 spectropolarimeter. UV-vis absorption spectra were measured on a UV-2550 spectrometer. The luminescence spectra and lifetimes were measured on an Edinburgh instruments Model FLS980 spectrometer. The absolute quantum yields were determined using an integrating sphere (150 mm diameter, BaSO$_4$ coating) of Edinburgh instruments. Magnetic data were measured by a Quantum Design MPMS-XL5 magnetometer. Diamagnetic corrections were estimated by using Pascal constants and background corrections by experimental measurement on sample holders.

Syntheses of complexes 1−10

Ln(*R*-pba)$_3$ was synthesized according to the reported literature with minor modifications.[16] A methanolic solution (1 ml) of *R*-pba (1.5 mmol, 246 mg) and CH$_3$ONa (1.5 mmol, 81 mg) was added into the water solution (20 ml) of LnCl$_3$·6H$_2$O (0.5 mmol, 187 mg), and the precipitate of Ln(*R*-pba)$_3$ was obtained. The white precipitate was collected and dried in vacuum. The acetonitrile solution of Ln(*R*-pba)$_3$ (0.05 mmol, 32 mg) and phen (0.05 mmol, 9.9 mg) was stirred at 60 °C for 2 h, and

2

the mixture was evaporated in an oven to obtain target solids (**1–10**). The crystals suitable for X-ray analysis were obtained by layering petroleum ether over the CHCl$_3$ solution of **1–10**. Yield: 40−50%. Observed/calculated elemental analyses and selected IR spectra data of **1–10** are listed in Table S1 (ESI). The enantiomers of complexes **1−10** {[Ln(*S*-pba)$_3$(phen)]$_2$} were synthesized by the same procedure except that the *R*-pba was replaced by the *S*-pba. Their characterization data including crystal data, selected bond lengths and angles, and selected IR spectra data are shown in Tables S12-S22 (ESI).

Crystallographic data and structure refinements

   The single-crystal X-ray diffraction data of **1−10** were collected on a Bruker D8 QUEST diffractometer using monochromated Mo-Kα radiation (λ = 0.71073 Å). The program *CrystalClear*[17] was used for the integration of the diffraction profiles. The structures were solved by direct method using the SHELXS program of the SHELXTL package and refined by full-matrix least-squares methods with SHELXL.[18] The non-hydrogen atoms were located in successive difference Fourier syntheses and refined with anisotropic thermal parameters on F^2. All hydrogen atoms of ligands were generated theoretically at the specific atoms and refined isotropically with fixed thermal factors. A summary of the crystallographic data, data collection and refinement parameters for **1−10** is provided in Tables 1−3.

<div align="center">(Insert Tables 1−3)</div>

Results and discussion

IR, UV-vis and CD spectra

   There are similar IR, UV-vis and CD spectra for all complexes due to their isostructural crystals. From the IR spectra (Table S1, ESI), the weak peak appeared at about 3445-3386 cm^{-1} can be attributed to the vibration of carboxylate group. There are two very strong peaks at around 1600 cm^{-1} and 1410 cm^{-1}, respectively, which are attributed to the stretching vibration of carbonyl group. There are a strong peak at 1515−1557cm^{-1}, a weak peak at 845 cm^{-1} and a medium peak at 731 cm^{-1}, which are attributed to the stretching vibration of pyridine rings and C-H groups of phen. There is a trend of shift to higher vibration frequency with the lanthanide contraction. From the UV-vis spectra (Fig. 1), the several peaks in the range of 200-320 nm can be attributed to the π-π* transitions of the ligands, which is further supported by the UV-vis spectra of these two organic ligands (Fig. S1, ESI). In order to confirm the

optical activity and enantiomeric nature, the circular dichroism (CD) spectra of **1**−**10** in CH$_3$CN solution were measured (Fig. 2). The CD spectra of complexes **1**−**10** (*R* enantiomers) exhibit a negative Cotton effect at around 265 nm, and positive dichroic signals centered at 220 and 280 nm, respectively, while the *S* enantiomers show Cotton effects of the opposite signals at the same wavelengths. The CD peaks can be assigned to the π-π* transition of the UV/vis absorption spectra of the corresponding complexes, which are centered at 220, 265 and 280 nm, respectively. The CD spectra further confirm the optical activity and enantiomorphous properties of these complexes. The intensity of the two peaks around 220-270 nm of all complexes in both the UV/vis spectra and the CD spectra is strongly varied with the concentrations in solution and the different lanthanide ions coordinated to the organic ligands. Because there are two 1,10-phenanthroline chromophores and six benzene chromophores of the *R*-pba ligands arranged in a chiral configuration in these dinuclear complexes, two or more electric dipole transition moments may be coupled with each other by a dipole–dipole interaction according to the exciton theory.[19] Consequentially, the degenerate excited states will split, therefore, the double peaks or shoulder peaks rather than the single peak around 225 and 260 nm in the UV/vis spectra can be observed for the benzene chromophor and the phen chromophore, respectively. All these peaks belong to the π-π* transitions of the ligands.

<div align="center">(Insert Fig. 1 and 2)</div>

Description of crystal structures

The single X-ray crystallography analyses reveal that the trend of the volumes of crystal cell follows the lanthanide contraction on the whole and the reason of the exception could be attributed to the existence of "gadolinium break effect (GBE)".[20] All the compounds are isostructural and crystallize in the chiral space group *P*2$_1$. As shown in Fig. 3a, each molecule of **1**−**10** consists of two Ln(III) ions, six *R*-pba ligands and two phen ligands. Each Ln(III) ion is nine-coordinated with one chelating *R*-pba group, five O atoms from four bridging *R*-pba ligands and two N atoms from the phen ligand. The two Ln(III) ions are bridged by four *R*-pba ligands with the *syn-syn*-μ_2-η^1:η^1 and *syn-syn*-μ_2-η^1:η^2 modes. Very interestingly, *R*-pba exhibits three different coordination modes in these complexes, which is relatively rare in the known complexes constructed by monocarboxylate ligands and feasible to construct much more complicated and fantastic frameworks with interesting properties (Scheme 2). The coordination environment of each Ln(III) ion can be described as a distorted monocapped square antiprism geometry. For the coordination environment of Ln1 ion (Fig. 3b), the atoms O8, O9, N1, N2 (below) and O3, O4, O5, O7 (top) form the

square planes, respectively. As shown in Fig. S2 (ESI), each complex is orderly stacked in a head-to-tail manner *via* the $\pi\cdots\pi$ interactions and forms a one-dimensional array. The separation between two adjacent and partially overlapping phen ligands is around 3.40–3.68 Å, suggesting the presence of the weak intermolecular $\pi\cdots\pi$ interactions.[21] The differences of π-π stacking interactions between **1-6** and **7-10** may be attributed to the distinct ionic radius. In the series from La1-La2 to Ho1-Ho2, the Ln−O and Ln−N bond lengths decrease with the atomic number of the Ln(III) ion increases, the La−O and La−N bond lengths are 2.444(5)–2.714(5) Å and 2.712(6)–2.731(5) Å, respectively, while the Ho−O and Ho−N bond lengths are 2.303(1)–2.592(10) Å and 2.501 (13)–2.597(13) Å, respectively. Moreover, the intra-molecular Ln1$\cdots$Ln2 separation decreases from 4.0975(4) Å for the La1-La2 to 3.9025(7) Å for the Ho1-Ho2. Thus, a series of dinuclear lanthanide clusters derived from chiral *R*-pba and phen ligands has been obtained.

<div align="center">(Insert Fig. 3 and Scheme 2)</div>

Luminescent properties

The photoluminescence properties of complexes **6, 8** and **9** in solid state at room temperature were measured. The excitation spectra of **6** at room temperature by monitoring 615 nm emission were exhibited in Fig. 4. It was clearly observed that the characteristics excitation peaks of the Eu(III) ion at 465, 395 and 375 nm correspond to the $^7F_0$ -$^5D_2$, $^5L_{6, 7}$ transitions, respectively. An intense broad absorption band centered at about 337 nm was observed, which indicates the existence of the charge transfer (CT) from O^{2-} to the Eu(III) ion. Complex **6** exhibits the characteristic transitions of the Eu^{III} ion under excitation at 337 nm. The peaks at 580, 590, 615, 650 and 700 nm are assigned to the $^5D_0{\rightarrow}^7F_0$, $^5D_0{\rightarrow}^7F_1$, $^5D_0{\rightarrow}^7F_2$, $^5D_0{\rightarrow}^7F_3$ and $^5D_0{\rightarrow}^7F_4$ transitions, respectively. And the most intense emitting band at 615 nm dominates the red emission light. The intensity of the $D_0{\rightarrow}^7F_2$ transition (electric dipole) is stronger than that of the $^5D_0{\rightarrow}^7F_1$ transition (magnetic dipole), indicating that the coordination environment of Eu(III) ion is asymmetric,[22] which is confirmed by the crystallographic structure analyses as shown above. In order to investigate the luminescence dynamic of the Eu(III) in **6**, the luminescent decay curves of $^5D_0{\rightarrow}^7F_2$ were measured at room temperature (excitation at 337 nm). The luminescence decay curves of **6** are shown in Fig. 5 in semilog scale. The decay curve for $^5D_0{\rightarrow}^7F_2$ (615 nm) of the Eu(III) ions can be well fitted into a single-exponential function as $I = A\exp(-t/\tau)$. The lifetime for $^5D_0$ energy level of the Eu(III) ions at room temperature is

about 1.62 ms. The single-exponential decay behavior of the activator is observed when the activator lies in the same coordination environment.[23] It is well known that the luminescence quantum yield is an important parameter for evaluating the luminescence properties of the phosphor. The absolute quantum yield can be defined as the integrated intensity of the luminescence signal divided by the integrated intensity of the absorption signal. The absolute quantum yield (45.6%) of **6** is determined by the average value of three measurements. These values (the lifetime and absolute quantum yield) are larger than those of Eu(III) complex $[Eu_2(L)_6(H_2O)_4]$ (HL= 4-(dibenzylamino)benzoic acid).[24] There is C=O oscillators (about 1600 cm^{-1}) and not -OH oscillators (about 3400 cm^{-1}) for **6**. Low phonon frequency for symmetrical C=O stretching, which improves radiative transition from the $^5D_0$ excited state of Eu(III) ions for **6.**

(Insert Fig. 4 and 5)

Fig. 6 shows the excitation spectra of complex **8** by monitoring the emission of the Tb(III) $^5D_4 \rightarrow {}^7F_5$ transition at 545 nm. It can be clearly seen that the excitation spectrum consists of a strong and broad band from 250 to 400 nm with a maximum at about 350 nm, which corresponds to the charge transfer state from O^{2-} to Tb(III). The shoulder peak at 379 nm is assigned as the transition from the $^7F_6$ ground state to the $^5D_4$ excited states of Tb(III). Excitation of **8** at 350 nm shows a very strong and characteristic emission band of the Tb(III) ion (Fig. 6). Furthermore, other bands are attributed to the $^5D_4 \rightarrow {}^7F_6$ (490 nm), $^5D_4 \rightarrow {}^7F_5$ (545 nm), $^5D_4 \rightarrow {}^7F_4$ (585 nm), and $^5D_4 \rightarrow {}^7F_3$ (620 nm) transitions, respectively. Notably, the most intense green emitting band arises from the $^5D_4 \rightarrow {}^7F_5$ transition of the Tb(III) ion. The decay curve of Tb(III) ($^5D_4$) by monitoring the $^5D_4 \rightarrow {}^7F_5$ transition (545 nm) in crystal phosphor **8** can also be fitted with the single exponential, and the lifetime of Tb(III) ($^5D_4$) is 1.08 ms (Fig. 7), which is similar to that of bright luminescent Tb(III) complex $[Tb_2(XA)_6(DMSO)_2(H_2O)_2]$ (HXA = xanthene-9-carboxylic acid, DMSO = dimethylsulfoxide).[25] The absolute quantum yield (34.9%) of **8** is determined by the average value of three measurements, which is larger than that of complex $[Tb_2(XA)_6(DMSO)_2(H_2O)_2]$.[25] There is no high phonon frequency for symmetrical O-H stretching, which decreases multi-phonon non-radiative transition from the $^5D_4$ excited state of the Tb(III) ions for **8**. This high quantum yield of **8** might find potential application in the field of light display systems.

(Insert Fig. 6 and 7)

For **9**, upon excitation at 335 nm at room temperature, it displays multiple

emission peaks at 375, 482, 575, 663, and 750 nm (Fig. 8). The first broad band centered at 375 nm is attributable to the reserved intra-ligand charge transfer (ILCT) emission of the *R*-pab ligand.[21] There are two strong emission bands at 482 and 575 nm, in which the blue (482 nm, $^4F_{9/2}{\rightarrow}^6H_{15/2}$) and yellow (575 nm, $^4F_{9/2}{\rightarrow}^6H_{13/2}$) light emission bands composite into the white light. The $^4F_{9/2}{\rightarrow}^6H_{13/2}$ transition is attributed to the hypersensitive transition with $J = 2$, which is strongly influenced by the coordination environment of the Dy(III) ion. The emission intensity of the $^4F_{9/2}{\rightarrow}^6H_{13/2}$ transition is stronger than that of the $^4F_{9/2}{\rightarrow}^6H_{15/2}$ transition, which indicates that the Dy(III) ion is in a lowly symmetric site. The ($^4F_{9/2}{\rightarrow}^6H_{13/2}$)/($^4F_{9/2}{\rightarrow}^6H_{15/2}$) emission ratio of the Dy(III) ion for **9** and the ($^5D_0{\rightarrow}^7F_2$)/($^5D_0{\rightarrow}^7F_1$) emission ratio of the Eu(III) ion for **6** exhibit the same trend. These results also prove that the local symmetry of the activator ions belongs to no inversion symmetry in the structures of [Ln(*R*-pba)$_3$(phen)]$_2$.

(Insert Fig. 8)

Magnetic properties

The magnetic properties of **7−10** were investigated by solid state magnetic susceptibility measurements in 2−300 K range at 1 kOe field and the isothermal field-dependent magnetizations *M(H)* at fields up to 50 kOe at 2 K. For complexes **7−10**, the $\chi_M T$ values at 300 K are 15.93, 22.26, 26.82 and 28.36 emu mol^{-1} K (Fig. 9), respectively, being close to the corresponding spin-only values expected for two isolated Ln(III) ions (C_{Gd} = 15.76 emu mol^{-1} K, C_{Tb} = 23.63 emu mol^{-1} K, C_{Dy} = 28.34 emu mol^{-1} K and C_{Ho} = 28.14 emu mol^{-1} K). For **7−10**, with the temperature decreasing, the $\chi_M T$ value stays nearly constant in the high temperature range and decrease quickly at very low temperatures to the minimum values (13.65, 15.84, 19.96 and 5.93 emu mol^{-1} K, respectively) at 2 K, which is likely due to crystal-field effects (*i.e.* thermal depopulation of the Ln(III) Stark sublevels) and/or the possible antiferromagnetic dipole–dipole interaction between the molecules. Fitting the data of χ_M^{-1} *vs.* *T* between 300 and 2 K to the Curie–Weiss law gives C = 16.04 emu mol^{-1} K (**7**), 22.67 emu mol^{-1} K (**8**), 27.32 emu mol^{-1} K (**9**) and 29.01 emu mol^{-1} K (**10**), and θ = −0.59 K, −2.47 K (**8**), −2.99 K (**9**) and −7.5 K (**10**) (Fig. S3, ESI). The small negative θ values of **7−10** are presumably caused by antiferromagnetic interaction and/or the crystal-field effect of the free Ln(III) ion.

(Insert Fig. 9)

The *M vs. H* curves (2 K) for **7−10** are shown in Fig. 10. For **7**, the magnetization increases fast and tends to 14.57 Nβ at 50 kOe. Below 35 kOe, the magnetization increases more slowly than that of the uncoupled Gd$_2$ system as the theoretical

Brillouin curve shows, which confirms the weak antiferromagnetic interaction between the Gd(III) ions (Fig. 10a). For **8–10**, the magnetizations increase quickly at very low field, reaching about 9.27, 13.51 and 4.46 Nβ at 10 kOe, respectively (Fig. 10b). In the high field region, the increase of magnetization is slow and linear, and the *M* values reach to 11.90, 15.76 and 11.12 Nβ at 50 kOe, respectively, being far away from the theoretical saturated values anticipated for two isolated Ln(III) ions, which may be attributed to the anisotropy of the polycrystalline samples and the depopulation of the Stark levels of the Ln(III) $^{2S+1}F_J$ ground state under the ligand-field perturbation, which produces a much smaller effective spin.

(Insert Fig. 10)

Conclusions

Ten new chiral Ln(III) dinuclear complexes based on *R*-2-phenylbutyric acid and 1,10-phenanthroline have been successfully prepared and structurally characterized. The single X-ray crystallography study reveals that all the complexes are isostructural and crystallize in the chiral space group *P*2$_1$. Magnetic studies show that **7-10** exhibit the antiferromagnetic coupling between the two Ln(III) ions. Interestingly, complexes **6**, **8** and **9** show strong solid state photoluminescent properties at ambient temperature, indicating that these complexes can be used as the efficient luminescent molecular materials. Our work demonstrate that the chiral carboxylate ligand can be successfully introduced into the lanthanide complexes in crystalline state showing luminescent properties, which suggests an effective approach to the chiral luminescent crystal materials.

Acknowledgements

Notes and references

[a]School of Metallurgy and Chemical Engineering, Jiangxi University of Science and Technology, Ganzhou 341000, Jiangxi Province, P.R. China. E-mail (H.-R Wen): wenherui63@163.com.

[b]Beijing National Laboratory for Molecular Sciences, Center for Molecular Science, Institute of Chemistry, Chinese Academy of Sciences, Beijing 100190, P.R. China. E-mail (C.-M. Liu): cmliu@iccas.ac.cn.

RSC Advances Accepted Manuscript

ᶜBeijing City Key Laboratory of Polymorphic Drugs, Center of Pharmaceutical Polymorphs, Institute of Materia Medica, Chinese Academy of Medical Sciences and Peking Union Medical College, Beijing 100050, P.R. China.

1　Y. Suzuki, Y. Ohkl and Y. Koizumi, *Coord. Chem. Rev.*, 1988, **92**, 29-43.

2　S.-J. Liu, J.-P. Zhao, W.-C. Song, S.-D. Han, Z.-Y. Liu and X.-H. Bu, *Inorg. Chem*., 2013, **52**, 2103-2109.

3　N. Zhao, S.-P. Wang, R.-X. Ma, Z.-H. Gao, R.-F. Wang and J.-J. Zhang, *J. Alloys Compd.*, 2008, **463**, 338-342.

4　S. Tanase, M. C. Mittelmeijer-Hazeleger, G. Rothenberg, C. Mathonière, V. Jubera, J. M. M. Smits and R. Gelde, *J. Mater. Chem.*, 2011, **21**, 15544-15551.

5　G. L. Law, K. L. Wong, K. K. Lau, S. Lap, P. A. Tanner, F. Kuo and W. T. Wong, *J. Mater. Chem.*, 2010, **20**, 4074-4079.

6　(a) J. Perles, M. Iglesias, C. Ruiz-Valero and N. Snejko, *J. Mater. Chem*., 2004, **14**, 2683-2689; (b) X. Li, T.-T. Zhang, Y.-L. Ju, C.-Y. Wang, Y.-Q. Li, L. Zhang and Q. Zhang, *J. Coord. Chem.*, 2007, **60**, 2121-2132.

7　(a) J. Rocha, L. D. Carlos, F. A. Almeida Paz and D. Ananias, *Chem. Soc. Rev.*, 2011, **40**, 926-940; (b) Y.-B. Lu, S. Jin, Z.-G. Zhou, S.-Y. Zhang, G.-T. Lou and Y.-R. Xie, *Inorg. Chem. Commum.*, 2014, **48**, 73-76; (c) W. J. Evans, D. G. Giarikos and J. W. Ziller, *Organometallics*, 2001, **20**, 5751-5758; (d) Z. Amghouz, S. García-Granda and J. R. García, *Inorg. Chem.*, 2012, **51**, 1703-1716.

8　(a) N. Ishikawa, M. Sugita, T. Ishikawa, S. Y. Koshihara and Y. Kaizu, *J. Am. Chem. Soc*., 2003, **125**, 8694-8695; (b) J. D. Rinehart and J. R. Long, *J. Am. Chem. Soc.*, 2009, **131**, 12558-12559; (c) M. A. Subhan, T. Suzuki, A. Fuyuhiro and S. Kaizaki, *Dalton Trans.,* 2003, **19**, 3785-3791; (d) Q. Gao, X.-Q. Wang and A. J. Jacobson, *Inorg. Chem.*, 2011, **50**, 9073-9082; (e) O. Kotova, S. Blasco, B. Twamley, J. O'Brien, R. D. Peacock, J. A. Kitchen, M. Martínez-Calvoa and T. Gunnlaugsson, *Chem. Sci.*, 2015, **6**, 457-471; (f) G. Bozoklu, C. Gateau, D. Imbert, J. Pécaut, K. Robeyns, Y. Filinchuk, F. Memon, G. Muller and M. Mazzanti, *J. Am. Chem. Soc.*, 2012, **134**, 8372-8375; (g) J. Gregoliński, R. Wieczorek and J.

Lisowski, *Eur. J. Inorg. Chem.*, 2011, 3717-3725; (h) Y.-L. Li, Qing-Yan Liu, Cai-Ming Liu, Yu-Ling Wang and Ling Chen, *Aus. J. Chem.*, 2015, **68**, 488-492; (i) C.-B. Han, Y.-L. Wang, Y.-L. Li, C.-M. Liu, Q.-Y. Liu, *Inorg. Chem. Comm.*, 2015, **58**, 91-94.

9   (a) J. M. Ribó, J. Crusats, F. Sagués, J. Claret and R. Rubires, *Science*, 2001, **292**, 2063-2066; (b) L. J. Prins, J. Huskens, F. de Jong, P. Timmerman and D. N. Reinhoudt, *Nature*, 1999, **398**, 498-502. (c) T. Verbiest, S.V. Elshocht, M. Kauranen, L. Hellemans, J. Snauwaert, C. Nuckolls, T. J. Katz and A. Persoons, *Science*, 1998, **282**, 913-915.

10   (a) E. Coronado, J. R. Galan-Mascaros, C. J. Gomez-Garcia and V. Laukhin, *Nature*, 2000, **408**, 447-449; (b) J. F. Scott, *Nat. Mater.*, 2007, **6**, 256-257; (c) R. Ramesh and N. A. Spaldin, *Nat. Mater.*, 2007, **6**, 21-29; (d) C.-F. Wang, D.-P. Li, X. Chen, X.-M. Li, Y.-Z. Li, J.-L. Zuo and X.-Z. Yo, *Chem. Commun.*, 2009, **45**, 6940–6942.

11   (a) J. Zhang, S. M. Chen, A. Zingiryan and X. H. Bu, *J. Am. Chem. Soc.,* 2008, **130**, 17246-17247; (b) G. Li, W. B. Yu and Y. Cui, *J. Am. Chem. Soc.*, 2008, **130**, 4582-4583; (c) B. F. Abrahams, M. Moylan, S. D. Orchard and R. Robson, *Angew. Chem., Int. Ed.,* 2003, **42**, 1848-1851.

12   (a) T. Tanaka, Y. Yasuda and M. Hayashi, *J. Org. Chem.,* 2006, **71**, 7091-7093; (b) D. J. Darensbourg and O. Karroonnirun, *Inorg. Chem.,* 2010, **49**, 2360-2371.

13   (a) I. Ojima, Catalytic Asymmetric Synthesis, second ed., Wiley-VCH, New York, 2000, p467-491; (b) J. Inanaga, H. Furuno and T. Hayano, *Chem. Rev.*, 2002, **102**, 2211-2226; (c) D. N. Dybtsev, A. L. Nuzhdin, H. Chun, K. P. Bryliakov, E. P. Talsi, V. P. Fedin and K. Kim, *Angew. Chem., Int. Ed.,* 2006, **45**, 916-920.

14   (a) E. Coronado, J. R. Galán-Mascarós, C. J. Gómez-García and J. M. Martinez-Agudo, *Inorg. Chem.*, 2001, **40**, 113-120; (b) C. Train, R. Gheorghe,V. Krstic, L. M. Chamoreau, N. S. Ovanesyan, G. L. J. A. Rikken, M. Gruselle and M. Verdaguer, *Nat. Mater.*, 2008, **7**, 729-734; (c) E. Coronado, J. R. Galán-Mascarós, C. J. Gómez-García and A. Murcia-Martínez, *Chem.– Eur. J.*, 2006, **12**, 3484-3492.

15   (a) R. S. Dickins, S. Aime, A. S. Batsanov, A. Beeby, M. Botta, J. I. Bruce, J. A. K. Howard, C. S. Love, D. Parker, R. D. Peacock and H. Puschmann, *J. Am. Chem. Soc.*, 2002, **124**, 12697-12705; (b) L. Croitor, E. B. Coropceanu, A. V. Siminel, V. C. Kravtsov and M. S. Fonari, *Cryst. Growth Des.,* 2011, **11**, 3536–3544.

16   R. Wang and Z. Zheng, Rare Earth Coordination Chemistry: Fundamentals and Applications, chapter 3: Rare Earth Complexes with Carboxylic Acids, Polyaminopolycarboxylic Acids, and Amino Acids, VCH, 2010.

17   Rigaku, Process-Auto. Rigaku Americas Corporation: The Woodlands, Texas, 1998.

18   G. M. Sheldrick, *SHELXL97*, *Program for Crystal Structure Refinement.* University of Göttingen: Göttingen, Germany, 1997.

19 (a) M. Ziegler and A. von Zelewsky, *Coordin. Chem. Rev.*, 1998, **177**, 257–300. (b) N. Berova, L. D. Bari and G. Pescitelli, *Chem. Soc. Rev.*, 2007, **36**, 914–931.

20 (a) Stéphane Rigault and Claude Piguet, *J. Am. Chem. Soc.*, 2000, **122**, 9304-9305; (b) Q.-B. Bo, Z.-X. Sun and W. Forsling, *CrystEngComm*, 2008, **10**, 232–238.

21   Z.-P. Deng, W. Kang, L.-H. Huo, H. Zhao and S. Gao, *Dalton Trans.,* 2010, **39**, 6276-6284.

22   Q.-Y. Yang, K. Wu, J.-J. Jiang, C.-W. Hsu, M. Pan, J.-M. Lehn and C.-Y. Su, *Chem. Commun.*, 2014, **50**, 7702-7704.

23   (a) F. Lei and B. Yan, *J. Solid State Chem.,* 2008, **181**, 855-862; (b) G. H. Jia, C. Y. Tu, J. F. Li, X. A. Lu, Z. Y. You, Z. J. Zhu and B. C. Wu, *J. Appl. Phys.,* 2005, **98**, 093525.

24 A. R. Ramya, M. L. P. Reddy, A. H. Cowley and K. V. Vasudevan, *Inorg. Chem.,*2010, **49**, 2407-2415.

25   R. Shini, S. Biju, M. L. P. Reddy, A. H. Cowley and M. Findlater, *Inorg. Chem.,* 2007, **46**, 11025-11030.

Table 1. Crystal data and refinement for the complexes **1−4**

Complex	**1**	**2**	**3**	**4**
formula	$C_{84}H_{82}La_2N_4O_{12}$	$C_{84}H_{82}Ce_2N_4O_{12}$	$C_{84}H_{82}N_4O_{12}Pr_2$	$C_{84}H_{82}N_4Nd_2O_{12}$
formula weight	1617.35	1619.78	1621.36	1628.02
T (K)	297(2)	298(2)	298(2)	295(2)
crystal system	Monoclinic	Monoclinic	Monoclinic	Monoclinic
space group	$P2_1$	$P2_1$	$P2_1$	$P2_1$
a (Å)	12.9648(8)	12.9263(7)	12.8915(6)	12.8651(6)
b (Å)	23.1129(13)	23.1494(14)	23.1403(11)	23.1584(10)
c (Å)	13.4817(8)	13.4675(8)	13.4533(6)	13.4478(6)
β (°)	109.069(2)	109.157(1)	109.2870(10)	109.4080(10)
V (Å^3)	3818.2(4)	3806.8(4)	3788.1(3)	3778.9(3)
Z, D_c (Mg/m^3)	2, 1.407	2, 1.413	2, 1.421	2, 1.431
μ (mm^{-1})	1.17	1.24	1.34	1.423
F (000)	1648	1652	1656	1660
R(int)	0.054	0.028	0.047	0.026
goodness of fit	1.045	1.060	1.009	1.108
final $R_1{}^a$, $wR_2{}^b$[I>2σ(I)]	0.0401, 0.0705	0.0277, 0.0520	0.0324, 0.0539	0.0330, 0.0598
R_1, wR_2 (all data)	0.0591, 0.0779	0.0354, 0.0552	0.0524, 0.0588	0.0412, 0.0635

$^aR_1 = \Sigma||F_o|-|F_c|| / \Sigma|F_o|$; $^bwR_2= [\Sigma[w(F_o{}^2-F_c{}^2)^2] / \Sigma w(F_o{}^2)^2]^{1/2}$.

Table 2. Crystal data and refinement for the complexes **5**−**8**

Complex	5	6	7	8
formula	$C_{84}H_{82}N_4O_{12}Sm_2$	$C_{84}H_{82}N_4O_{12}Eu_2$	$C_{84}H_{82}N_4O_{12}Gd_2$	$C_{84}H_{82}N_4O_{12}Tb_2$
formula weight	1640.24	1643.46	1654.04	1657.38
T (K)	299(2)	298(2)	299(2)	299(2)
crystal system	Monoclinic	Monoclinic	Monoclinic	Monoclinic
space group	$P2_1$	$P2_1$	$P2_1$	$P2_1$
a (Å)	12.810(2)	12.7972(17)	12.8326(6)	12.8517(15)
b (Å)	23.160(4)	23.189(3)	22.9406(10)	22.976(3)
c (Å)	13.434(2)	13.4405(18)	13.4767(6)	13.4781(15)
β (°)	109.337(4)	109.241(3)	109.0530(10)	109.129(3)
V (Å^3)	3761.0(10)	3765.8(9)	3750.0(3)	3760.1(7)
Z, D_c (Mg/m^3)	2, 1.448	2, 1.449	2, 1.465	2, 1.464
μ (mm^{-1})	1.611	1.715	1.818	1.930
F (000)	1668	1672	1676	1680
R(int)	0.029	0.023	0.028	0.031
Goodness of fit	1.035	1.240	1.058	1.062
final R_1^a, wR_2^b [I>2σ(I)]	0.0324, 0.0552	0.0377, 0.0784	0.0295, 0.0483	0.0296, 0.0686
R_1, wR_2 (all data)	0.0457, 0.0590	0.0426, 0.0831	0.0402, 0.0511	0.0315, 0.0711

$^aR_1 = \Sigma||F_o|-|F_c|| / \Sigma|F_o|$; $^bwR_2= [\Sigma[w(F_o^2-F_c^2)^2] / \Sigma w(F_o^2)^2]^{1/2}$.

Table 3. Crystal data and refinement for the complexes **9−10**

Complex	9	10
formula	$C_{84}H_{82}N_4O_{12}Dy_2$	$C_{84}H_{82}N_4O_{12}Ho_2$
formula weight	1664.54	1669.40
T (K)	296(2)	301(2)
crystal system	Monoclinic	Monoclinic
space group	$P2_1$	$P2_1$
a (Å)	12.8518(8)	12.819(3)
b (Å)	22.9659(14)	22.916(4)
c (Å)	13.4550(8)	13.425(3)
β (°)	109.120(2)	109.174(4)
V (Å^3)	3752.2(4)	3725.0(12)
Z, D_c (Mg/m^3)	2, 1.473	2, 3.986
μ (mm^{-1})	2.041	2.17
F (000)	1684	1688
R(int)	0.046	0.054
goodness of fit	1.098	0.966
final $R_1{}^a$, $wR_2{}^b$ [I>2σ(I)]	0.0983, 0.2081	0.0419, 0.0488
R_1, wR_2 (all data)	0.1024, 0.2098	0.0800, 0.0551

$^aR_1 = \Sigma||F_o|-|F_c|| / \Sigma|F_o|$; $^bwR_2= [\Sigma[w(F_o{}^2-F_c{}^2)^2] / \Sigma w(F_o{}^2)^2]^{1/2}$.

14
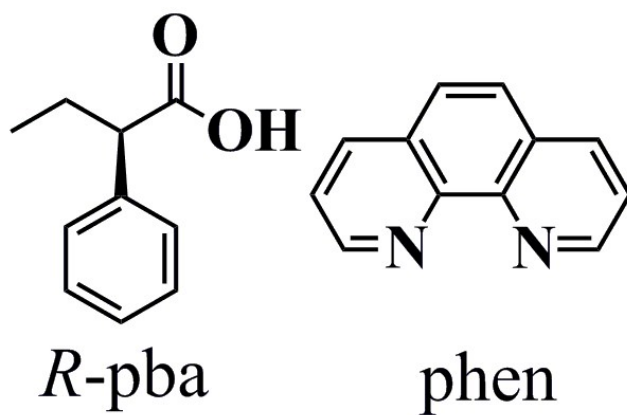
Scheme 1. The ligands used for the construction of target complexes.
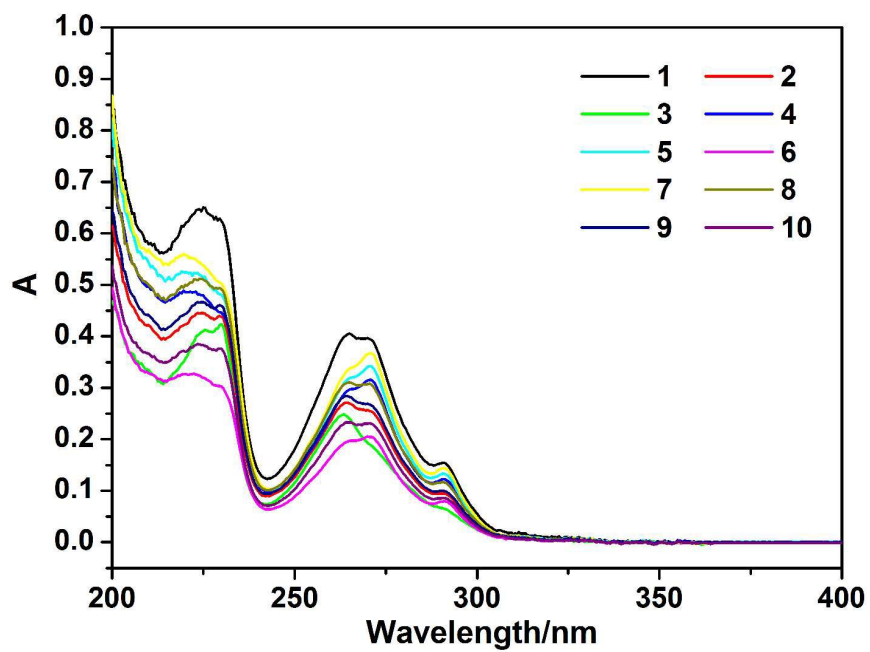
Fig. 1. UV-vis absorption spectra of **1−10** in CH$_3$CN solution.
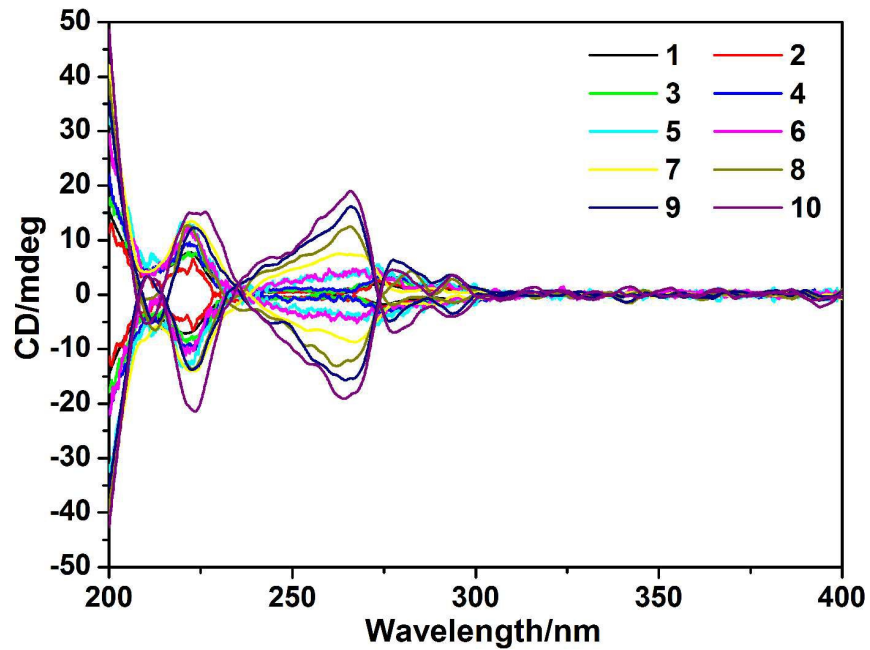
Fig. 2. Circular dichroism spectra of **1−10** enantiomers in CH$_3$CN solution.

(a)

(b)
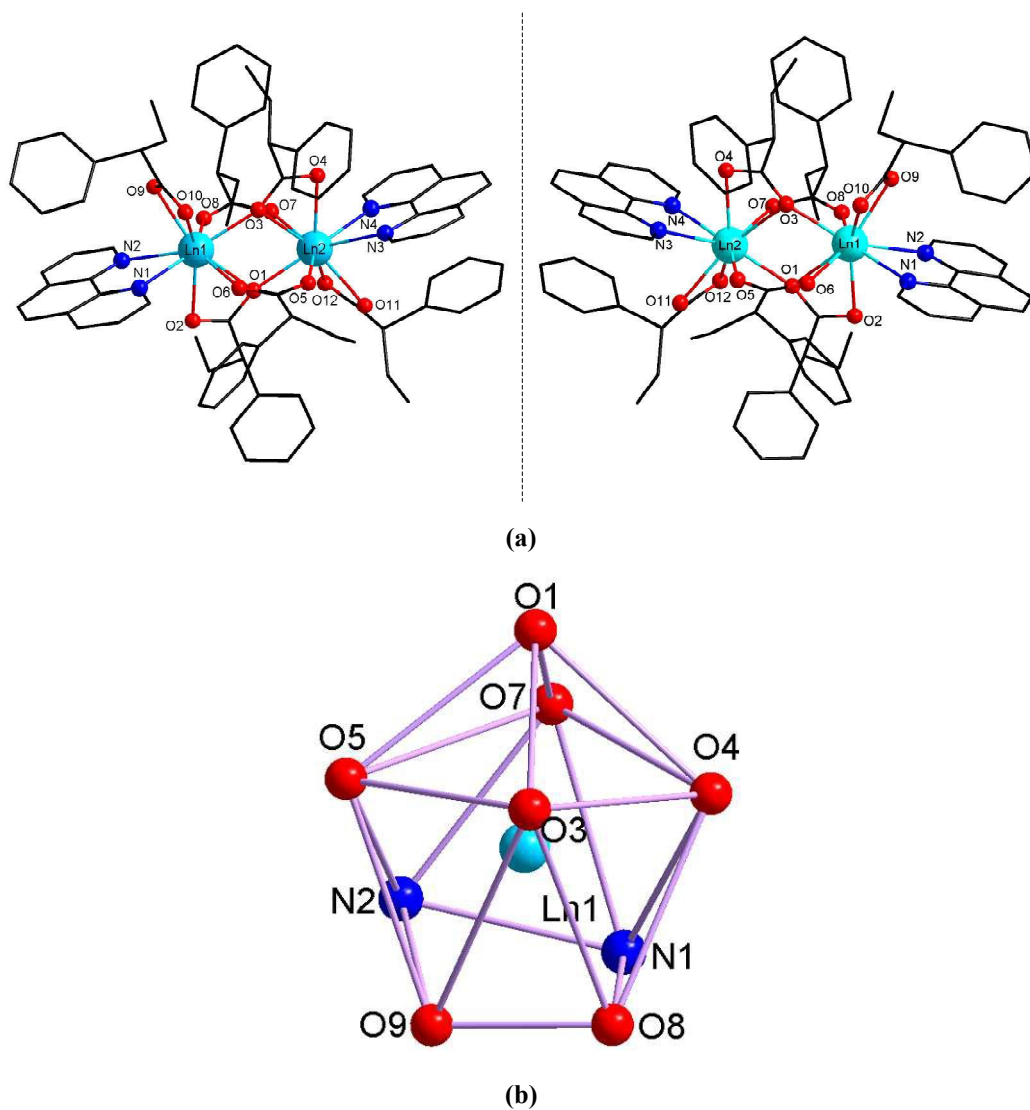
Fig. 3. (a) View of the molecular structure for [Ln(*R*-pba)$_3$(phen)]$_2$ and its enantiomer (all the hydrogen atoms omitted for clarity); (b) The coordination polyhedron around the Ln1 atom.
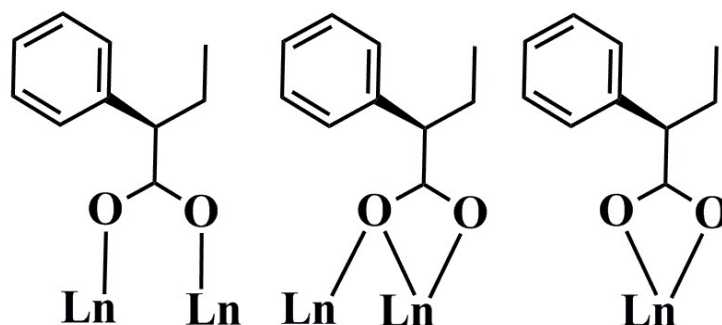
Scheme 2. The coordination modes of *R*-pba ligand in complexes **1–10**.
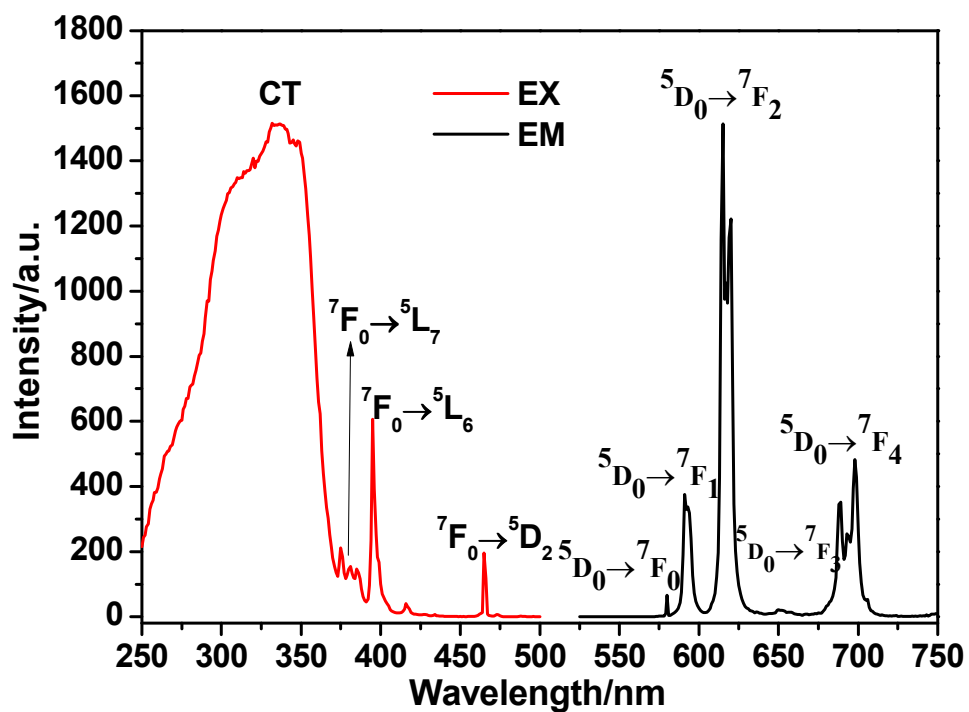
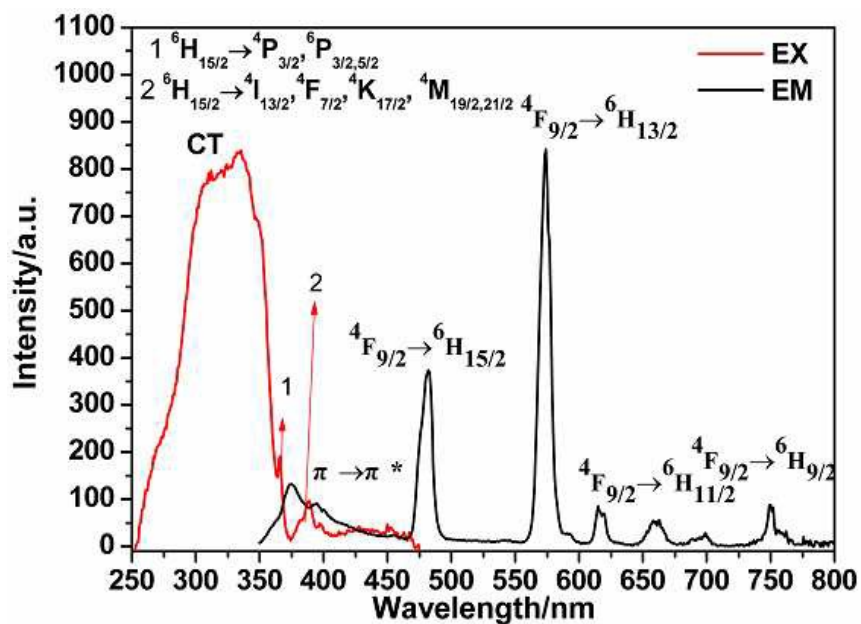**Fig. 4.** Excitation spectrum (λ_{em}= 618 nm) and emission spectra (λ_{ex}= 337 nm) for complex **6**.
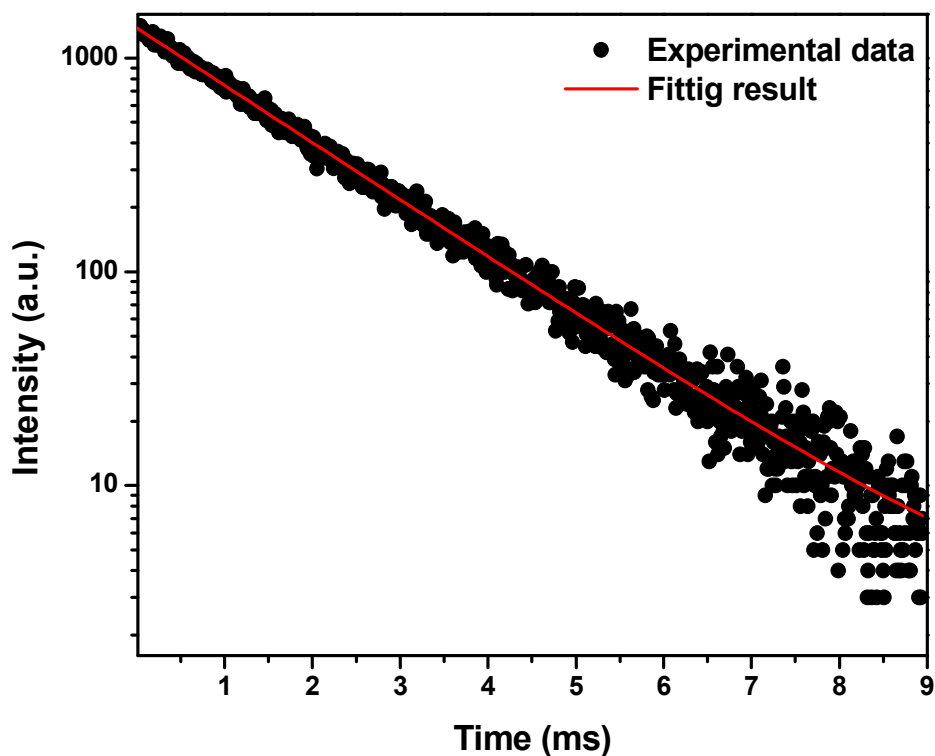
Fig. 5. Decay curve of complex **6** (excitation at 337 nm) at room temperature.
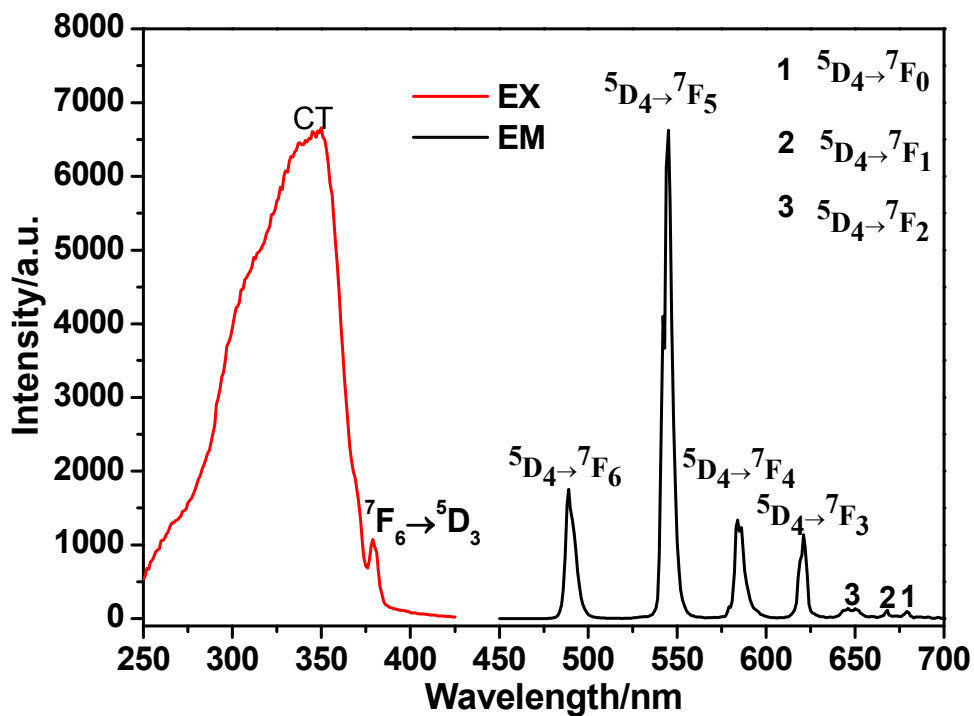
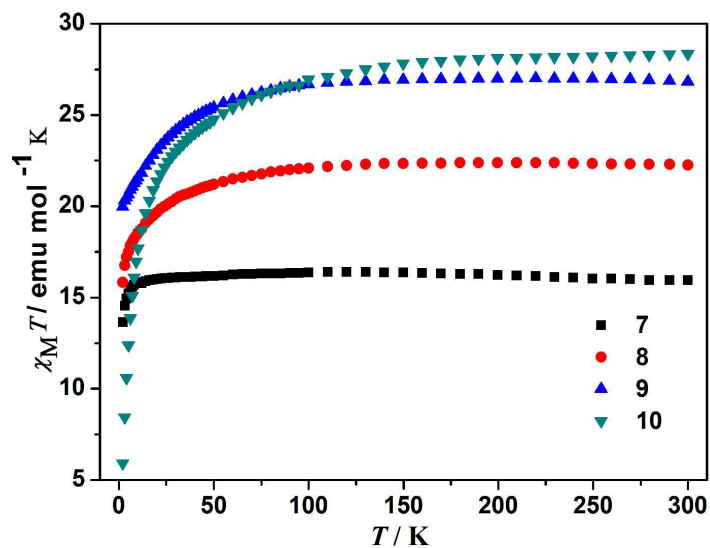**Fig. 6.** Excitation spectrum (λ_{em}= 546 nm) and emission spectra (λ_{ex}= 350 nm) for complex **8**.
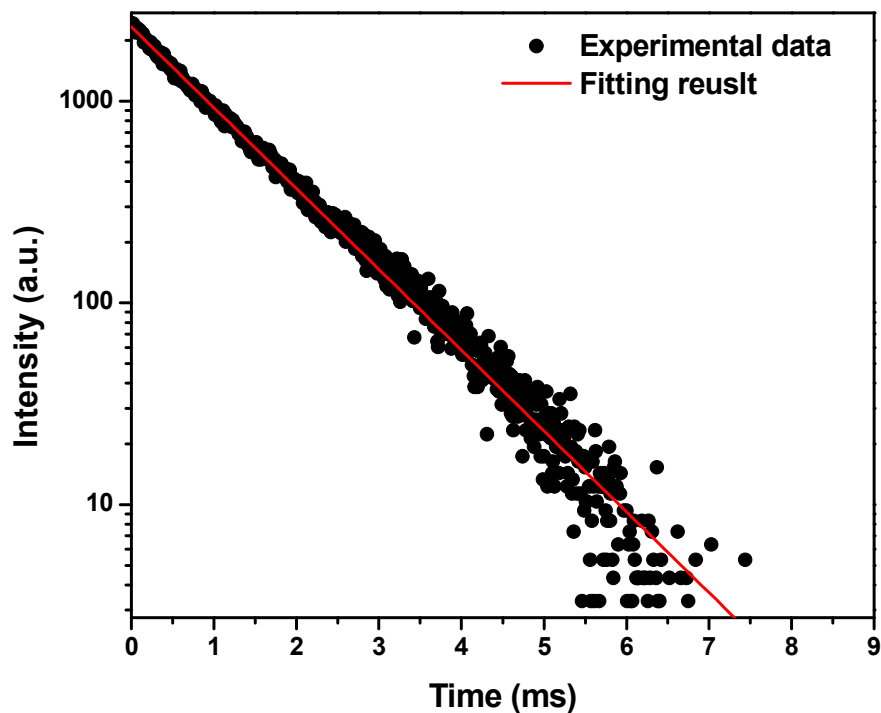
Fig. 7. Decay curve of complex **8** (excitation at 350 nm) at room temperature.

Fig. 8. Excitation spectrum (λ_{em}= 575 nm) and emission spectra (λ_{ex} = 335 nm) for complex **9**.
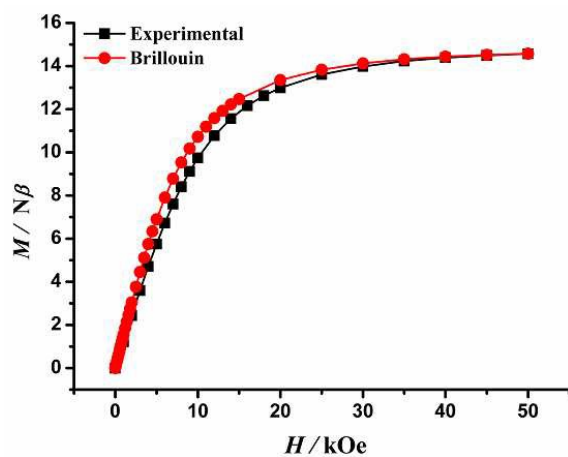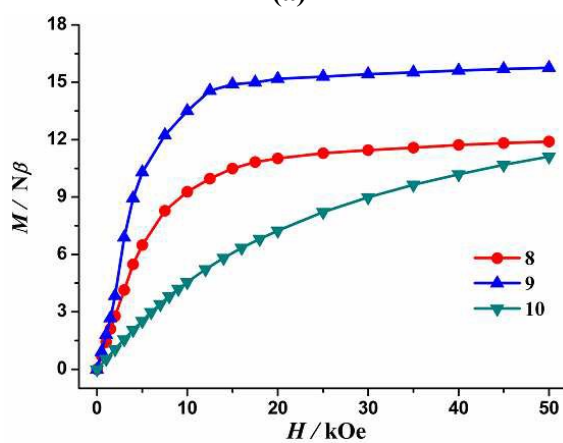
Fig. 9. Temperature dependence of magnetic susceptibilities in the forms of χ_MT for complexes **7−10**.

(a)

(b)

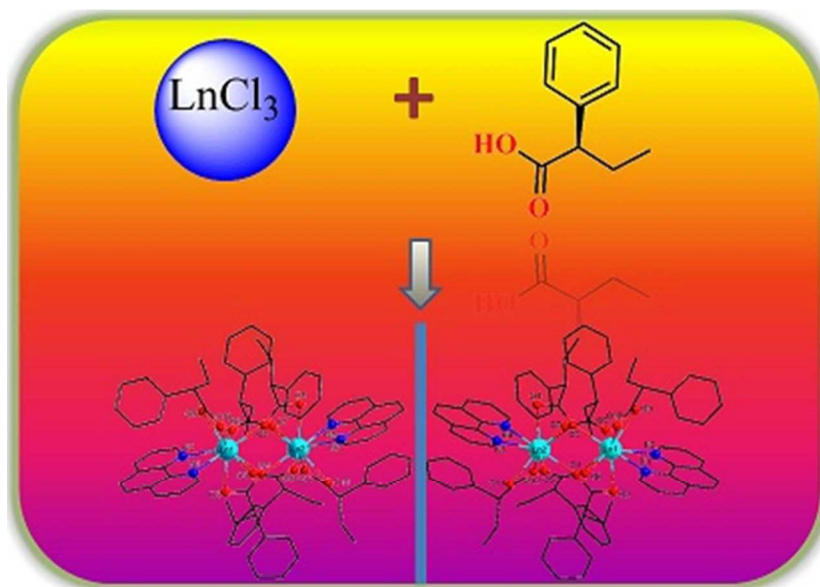**Fig. 10.** Field dependence of the magnetizations for **7** (a) and **8−10** (b) at 2 K.

<div style="text-align:center">**Graphic Abstract**</div>

Homochiral luminescent lanthanide dinuclear complexes derived from a chiral carboxylate

He-Rui Wen,* Xin-RongXie, Sui-Jun Liu, Jun Bao, Feng-Feng Wang, Cai-MingLiu* and Jin-Sheng Liao

A family of chiral Ln$_2$ clusters based on a chiral monocarboxylate ligand has been successfully constructed *via* diffusion method, and Eu, Tb and Dy analogues display good luminescent properties.